EURASIAN PHYSICAL TECHNICAL JOURNAL

2024, Volume 21, No. 3 (49)

https://doi.org/10.31489/2024No3/21-28

Received: 13/04/2024 Revised: 17/07/2024 Accepted: 17/09/2024 Published online: 30/09/2024
Research Article

UDC 537.534

OPTIMIZING THE INFLUENCE OF DOPING AND TEMPERATURE ON THE ELECTROPHYSICAL FEATURES OF P-N AND P-I-N JUNCTION STRUCTURES

Abdullayev J.SH.[1,2], Sapaev I.B.[1,3]

[1] National Research University "TIIAME", Tashkent, Uzbekistan
[2] Tashkent International University, Tashkent, Uzbekistan
[3] Western Caspian University, Scientific researcher, Baku, Azerbaijan
*Corresponding authors: j.sh.abdullayev6@gmail.com

Abstract. *In this paper, we investigate the effects of doping and temperature (at 300 K and 400 K) on the characteristics of Silicon (Si) and Gallium Arsenide (GaAs) p-n and p-i-n homojunction structures, utilizing doping concentrations of* $p^+ = n^+ = 2 \cdot 10^{17}$ *and* $p = n = 10^{16}$ cm^{-3} *through numerical calculation and modeling. Furthermore, we have analyzed three different cases: A) p-n, B)* p^+*-n, and C) p-*n^+*, to examine their influence on the distributions of space charge, potential, electric field, minority charge carriers, and the I-U curve at 300 K. It can be seen from the results that in case A, the recombination process is not observed at a lower voltage in the symmetrical p-n junction compared to than case B and C asymmetrical p-n junction. The voltage-temperature characteristics of the prepared samples were then measured at a temperature of 300K. I-U curve at 300 K. Calibration of the Si p-n homojunction structures is performed using experimental data to validate the proposed model. With the help of this constructed complex model, the influence of various geometrical changes, such as the radial p-n transition, on electrophysical properties will be examined in our next work.*

Keywords: Space charge density, doping concentration, modeling, calibration, optimization.

1. Introduction

In today's world, there is a growing demand for electronic devices that are integral to our daily lives. This surge in demand underscores the necessity for semiconductor electronic devices, prompting extensive scientific exploration in this field. Despite this demand, the outcomes of both theoretical and practical scientific investigations often fall short of meeting expectations.

Over five decades ago, scientific research delved into the initial p-n junction structures [1], yet several issues remain unresolved. Subsequent studies have theoretically examined the charge distribution within these junctions [2], though temperature variations have not been fully explored. Recombination mechanisms have been inferred solely from volt-ampere characteristics, neglecting by coordinate distribution of recombination rates [3]. Various devices, including solar cells [4], thermos sensors [5], diodes [6], and transistors [7], utilize p-n junction structures, while p-i-n junctions prove more effective for photodiodes and LEDs.

The characteristics and performance of p-i-n and p-n junction diodes are intricately tied to carrier behavior within the junction formed at the interface between p-type and n-type materials. These junctions serve as fundamental building blocks for various devices, with analysis techniques applicable to broader electronic problems. The kinetic processes of electrons and holes at p-n and p-i-n junctions are elucidated through two mechanisms: drift-diffusion and recombination-generation. The ideality factor, theoretically

ranging from 1 to 2, distinguishes between these mechanisms [8]. However, experimental data often indicate ideality factors exceeding 2 [9]. This study aims to explore the relationship between forward voltage and the ideality factor across different thicknesses of the i-layer. By modeling and analyzing the electrophysical properties of these junctions, semiconductor electronic devices can operate optimally with minimal energy consumption. Furthermore, such modeling enables understanding of quantum effects as semiconductor devices scale down from micro to nanoscale, facilitating analysis of external influences on optimal operational modes. Utilizing software platforms such as Synopsys Centaurus Device [10], Keysight ADS [11], SPICE [12], COMSOL Multiphysics [13], MATLAB [14], SCAPS1D [15], Numerical [16], and others addresses this need, facilitating comprehensive modeling of semiconductor electronic devices.

In this work, we study and simulate semiconductor p-n and p-i-n junctions based on GaAs and Si. Our research aims to understand the mechanisms that control current transport and the physical distribution of electrons within these junctions. Building upon these considerations, this work model p-n and p-i-n junction structures based on Si and GaAs under different forward voltages, doping concentrations, and temperatures. Section 2 discusses material and geometrical parameters, along with methodologies employed. Section 3 presents our model's results, and Section 4 summarizes our findings

2. Experimental measurements vs. device simulations

2.1 Theory and material parameters

The current mechanism in p-n or p-i-n junction semiconductor structures often involves the use of five fundamental expressions. These expressions play a decisive role in determining the distribution of the electric field and potential, which are derived from the Poisson equation (1). To perform this analysis, it is important to establish the charge distribution, usually represented by the concentration distribution.

$$\frac{dE(x)}{dx} = -\frac{d^2\varphi(x)}{dx^2} = \frac{q}{\varepsilon\varepsilon_0}(p - n + N_D - N_A) \tag{1}$$

From this expression, by substituting the electric field and potential distributions found when solving the differential equation into expressions (2) and (3), we derive expression (4) for the relationship between current and voltage for an ideal diode.

$$\frac{\partial n}{\partial t} = G_{net,n} - R_{net,n} + \frac{1}{q}\cdot\Delta J_n \tag{2a}$$

$$\frac{\partial p}{\partial t} = G_{net,p} - R_{net,p} - \frac{1}{q}\cdot\Delta J_p \tag{2b}$$

Equations (2a) and (2b), which detail the behavior of excess carriers within a semiconductor volume for electrons and holes, respectively, arising from phenomena such as generation, recombination, drift, and diffusion, are referred to as continuity equations.

$$J_n = J_{n,drift} + J_{n,diff} = q(n\mu_n E + D_n\frac{dn}{dx}) \tag{3a}$$

$$J_p = J_{p,drift} + J_{p,diff} = q(p\mu_p E - D_p\frac{dp}{dx}) \tag{3b}$$

The transport equations for electrons and holes in semiconductors can be formulated to include both diffusion and drift terms, represented as equations (3a) and (3b) respectively.

$$J = J_0(\exp(\frac{qU_{p-n}}{mkT}) - 1) \tag{4}$$

Where J_0 represents the saturation current, m denotes the ideality factor. m=1 corresponds to the drift-diffusion current loading mechanism at the source, while m=2 signifies the generation-recombination current carrier mechanism. (4) We can observe the expression values in figures 4 and 5.

To find the electric field, we integrate the expression (1) and obtain the electric field expression under the following conditions. (5a) and (5d) represent the quasi-neutral (QNR) fields in p-type and n-type regions, respectively, where the field is zero. (5b) and (5c) denote the depleted fields in p-type and n-type regions, respectively, where the electric field behaves like a linear function of distance. The four fields are depicted in Figs. 2 a), b), c), and d), respectively, with varying values

$$E(-\infty < x \le x_p) = 0 \quad (5a)$$

$$E(x_p < x < 0) = \frac{qN_A}{\varepsilon\varepsilon_0}(x + x_p) \quad (5b)$$

$$E(0 < x < x_n) = -\frac{qN_D}{\varepsilon\varepsilon_0}(x - x_n) \quad (5c)$$

$$E(x_n \le x < \infty) = 0 \quad (5d)$$

Where is ε permittivity dielectric constant, which is ε=11.9 for Si, ε=13 for GaAs, the electric field helps in separating the majority carriers injected into the opposite semiconductor regions due to diffusion or drift. Electrons move towards the positively charged region (p-type) and holes move towards the negatively charged region (n-type). The magnitude and distribution of the electric field affect the rate of carrier recombination and hence the current flow across the junction. Understanding the electric field helps in analyzing the current-voltage characteristics and overall performance of semiconductor devices like diodes and transistors. In optoelectronic devices like photodiodes and solar cells, the electric field assists in the separation of photo-generated electron-hole pairs, contributing to the device's efficiency. Electro field distribution together with the injection process is also important.

Injection of majority carriers (electrons from the n-type region and holes from the p-type region) across the junction occurs when the p-n junction is under forward bias. Injection affects the behavior of the p-n junction diode. Under forward bias, injection leads to a reduction in the width of the depletion region, facilitating the movement of majority carriers and allowing current to flow easily. In contrast, under reverse bias, injection is suppressed, and the depletion region widens, preventing significant current flow. Injection in a p-n junction is essential for controlling current flow, determining device characteristics, influencing carrier recombination, and enabling the operation of various semiconductor devices, particularly diodes and optoelectronic devices. The change in concentration of electrons on the p-side and holes on the n-side the quasi-neutral (QNR) fields expressed as:

$$\Delta n_p(x) = n_p(x) - n_{p0} = n_{p0}[\exp(\frac{qU_{p-n}}{kT}) - 1]\exp(\frac{x_p + x}{L_n}) \quad x < -x_p \quad (6a)$$

$$\Delta p_n(x) = p_n(x) - p_{n0} = p_{n0}[\exp(\frac{qU_{p-n}}{kT}) - 1]\exp(\frac{x_n - x}{L_p}) \quad x_n > x \quad (6b)$$

Where L_n, L_p are diffusion length electron and holes respectively, To calculate the various junction parameters it is important to define some concentration terms. On the p-side, let N_A be the concentration of the acceptors. If n_i is the carrier concentration, then the electron and hole concentrations on the p side are defined as $p_{p0}(-x_p < x < 0) = N_A$, $n_{p0}(-x_p < x < 0) = \frac{n_i^2}{N_A}$. Similarly, on the n-side, with donor concentration of N_D, the electron and hole concentration are as we move across the device is shown in Figure 3.

$$n_{n0}(0 < x < x_n) = N_D, \; p_{n0}(0 < x < x_n) = \frac{n_i^2}{N_D}.$$

$$\Delta n_p(x) = n_p(x) - n_{p0} = N_D[\exp(\frac{qU_{p-n}}{kT}) - 1] \quad x = -x_p \quad (7a)$$

$$\Delta p_n(x) = p_n(x) - p_{n0} = N_A[\exp(\frac{qU_{p-n}}{kT}) - 1] \quad x_n = x \quad (7b)$$

2.2 Device simulations

For the chosen model, geometric dimensions of a=10 μm, b=8 μm, and c=6 μm were selected. The following distinctions are made within the electrophysical models: the gap width varies with temperature [17], and the mobility of electrons and holes changes with temperature and concentration [18]. Additionally, Shockley-Read-Hall (SRH) recombination also varies with temperature and doping concentration [19].

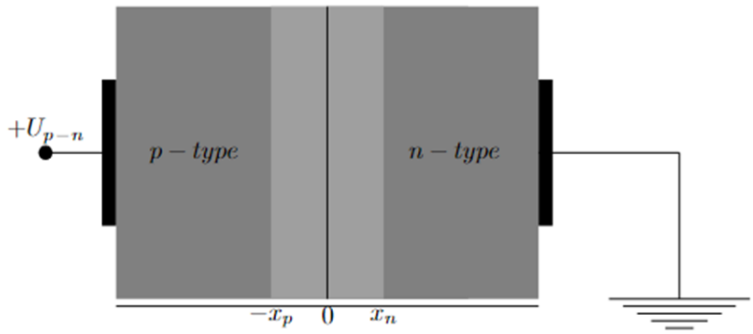

Fig. 1. This schematic depicts a 2D cross-section of our model planar p-n junction. The light grey area signifies the depletion region, while the dark grey area represents the quasi-neutral (QNR) fields in the p-type and n-type regions, respectively, based on both Si and GaAs materials.

The electric field distribution in this chosen model is illustrated in Figure 2, while the minority charge carriers are depicted in Figure 3. Additionally, the I-U characteristics are presented in Figures 4 and 5. The current-voltage *I-U* characteristic was studied at a voltage of +1 V for Si and +1.5 V for GaAs when the selected model was appropriately connected. The voltage supplied from the external source equals the p-n junction voltage. In this model, doping concentration is selected in three cases as follows: A) p-n, B) p^+-n, and C) p-n^+. After establishing the mathematical framework to describe a physical or engineering problem, such as through calculation geometry, the next step involves discretizing the problem domain into smaller elements using a finite-element grid. These elements break down the area of interest into manageable parts, often referred to as finite elements, with specific properties and behaviors. Each finite element grid node represents a point within the problem domain where the solution to the problem is evaluated or approximated. The solution typically involves determining scalar or vector fields, which represent physical quantities or properties of interest, at these nodes. Interpolation methods play a crucial role in finite-element analysis, allowing the estimation of values not only at the grid nodes but also at any point within the computational domain. This means that the behavior of the investigated function can be approximated or extrapolated at arbitrary locations, providing a comprehensive understanding of the system's behavior beyond the discrete grid points.

2.3 Experimental measurements

To calibrate and verify the theoretical and modeling analytical data presented above, an experimental sample was taken. In this case, an epitaxial layer of n-type silicon doped with Boron with a thickness of 30 μm and a concentration of $5 \cdot 10^{15}$ cm^{-3} is placed on a p-type silicon substrate doped with Phosphorus with a thickness of 280 μm and a concentration of $3 \cdot 10^{16}$ cm^{-3} grown and prepared based on the resulting silicon p-n structure. The experimental sample was prepared by depositing an aluminum layer on the contacts using the thermal sputtering method under vacuum conditions. The voltage-temperature characteristics of the prepared samples were then measured at a temperature of 300K. I-U curve at 300 K. Calibration of the Si p-n homojunction structures is performed using experimental data to validate the proposed model. The current-voltage characteristics of the sample were measured using current sources Б5-46М and Б5-47М, with a voltage step of 0.05 V during the experiment. Voltage was measured with a universal voltmeter Щ301-1, and current with a universal electronic device Щ300. The results of the experiment and the model are depicted in Fig. 4, where the I-U curve was concurrently measured for the GaAs material in this model.

3. Results and discussion

3.1 Distributions by distance

The electric field is a crucial parameter in various applications. Studying the dependence of field distribution on external parameters is essential because the field and potential distributions play significant roles in thermal sensors and photosensors. It can be observed from the second picture that the electric field is zero in both the p-type and n-type quasi-neutral regions (QNRs), as indicated by equations (5a) and (5d) respectively. In three cases as follows: A) p-n, B) p^+-n, and C) p-n^+, According to expressions (5a) and (5d), the depleted fields in p-type and n-type regions behave as linear functions of the electric field distance.

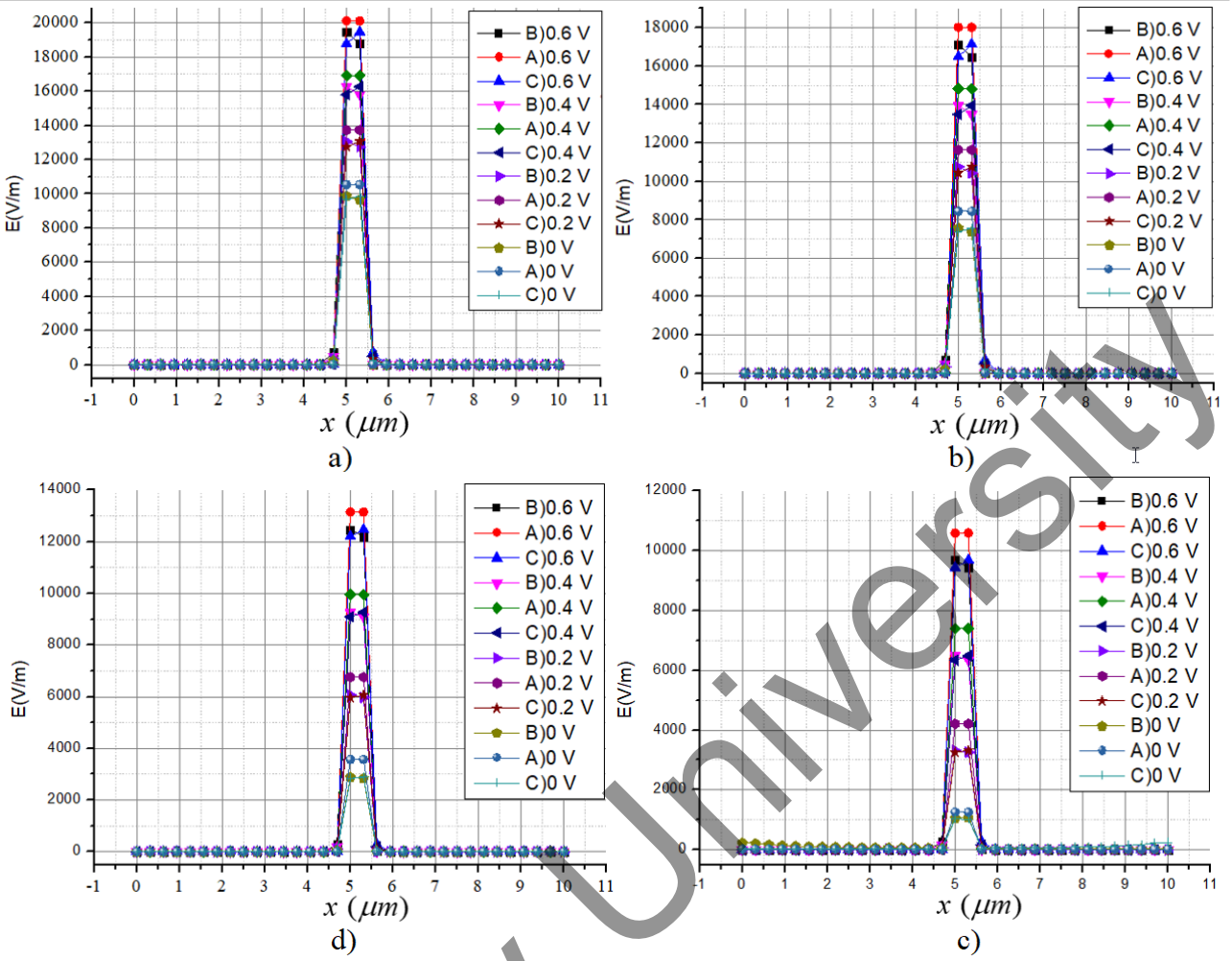

Fig.2. Electric field E(x) across a p-n junction a) 300 K b) 400 K based on GaAs, d)300 K c) 400 K based on Si.

The diffusion of minority charge carriers is called the injection process, and this injection depends on various external factors. Figure 3 shows the distance distribution of injected minor charge carriers. Adjusting the values of these fields alters the configurations shown in Figures 2 and 3. Moreover, at elevated temperatures, the field diminishes, reflecting characteristics specific to Si and GaAs. In Figure 3, it is evident that there is a close correspondence between the theoretical (7a), 7b) predictions and the outcomes generated by our model. This alignment highlights the robustness and accuracy of our model in capturing the underlying principles elucidated by the theoretical framework. It is assumed to be derived using the same process for electron density in p-QNR. Minority holes density in n-QNR, Minority electron density in p-QNR. Minority charge density dependent on voltage both Si and GaAs. The potential barrier is 0.82V for Si and 1.27V for GaAs.

3.2 Current-voltage characteristics

In this section, we delve into the classification and VAX results yielded by our innovative new model. Figure 4 shows a) the experiment and our new model in one graph for calibration, and b) VAX when our new model is used on GaAs material. Results can be seen to match with high accuracy.

The analysis of Figure 5 reveals qualitative homogeneity but quantitative disparities in the current transfer mechanism between cases A) and C), while case B) displays noticeable deviations in both qualitative and quantitative traits. Specifically, in case B), the drift-diffusion mechanism remains consistent up to the specified direct switching voltage for both Si and GaAs materials.

Figure 4 illustrates the semi-log current-voltage (I-V) characteristics for a p-n junction based on GaAs (a) and Si (b) materials, showcasing different forward voltage scenarios: A) p-n, B) p^+-n, and C) p-n^+.

In Figure 5a, it's evident that for cases A) and B), recombination predominates from a voltage delay of 0.2 V to 0.9 V in GaAs. Subsequently, from 0.9 V to 1.2 V, the drift-diffusion mechanism takes precedence.

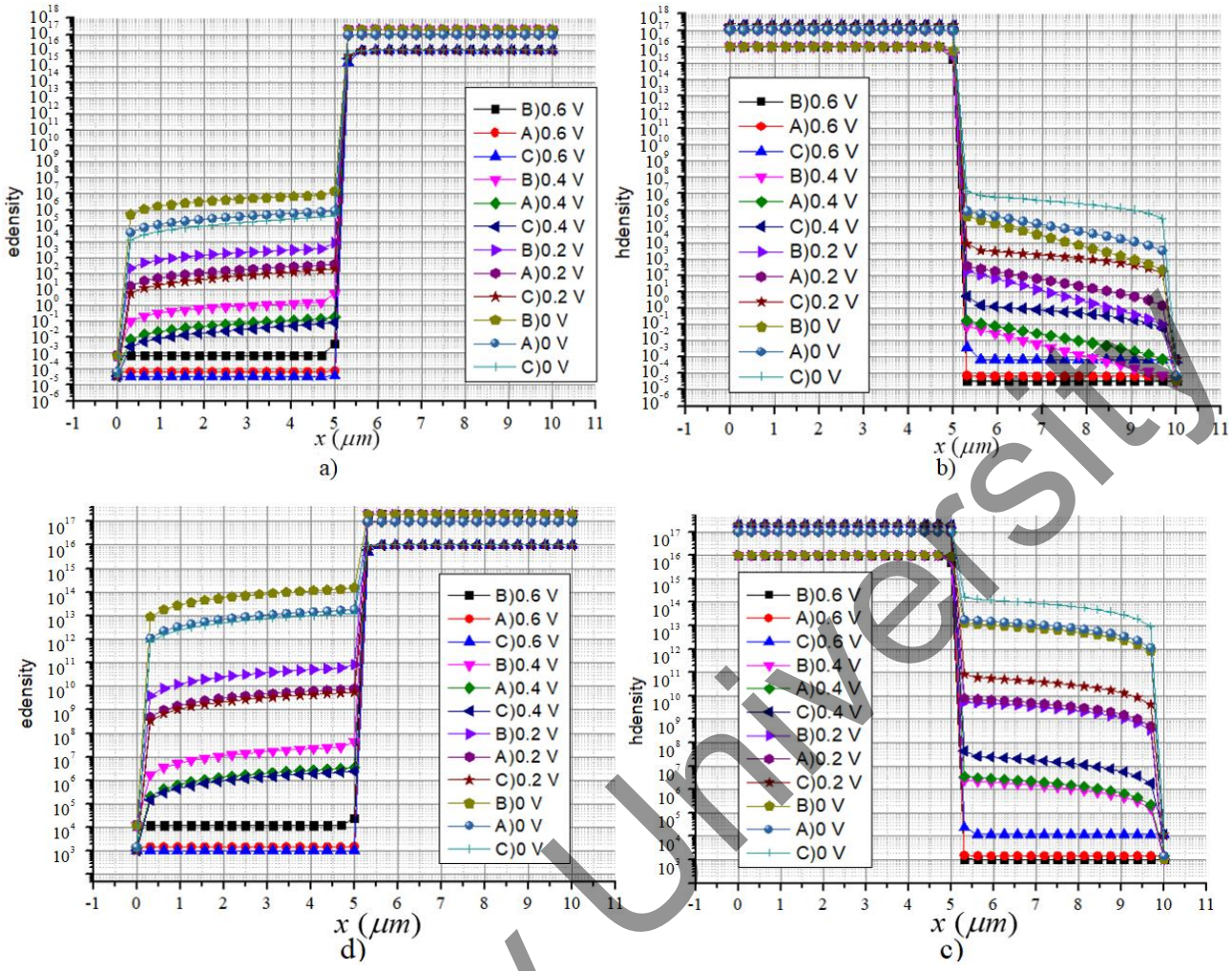

Fig.3. a) minority electrons density in n-QNR, b) minority holes density in p-QNR based on GaAs, a) minority holes density in n-QNR, b) minority electron density in p-QNR based on Si at 300 K at different voltage.

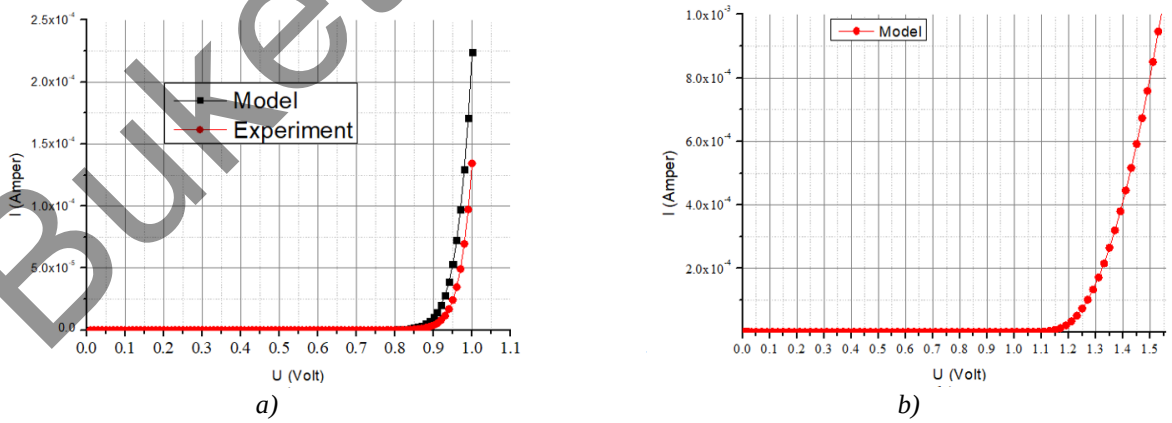

Fig. 4. Current-voltage characteristics for a p-n junction based on a) GaAs, b) Si forward voltage (Volts).

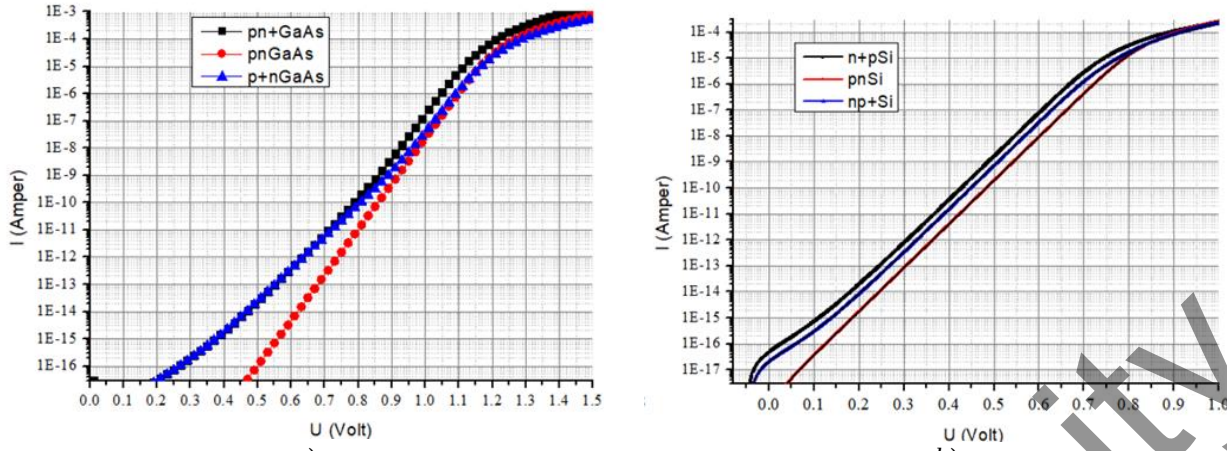

a) *b)*

Fig. 5. Semi-logarithmic current-voltage characteristics for a p-n junction based on a) GaAs, b) Si forward voltage (Volts).

Beyond 1.2 V, series resistance values and high injection processes are observable, explained by recombination, where minority charge carriers migrate from the emitter to the base region. Furthermore, Figure 5 illustrates that GaAs exhibit higher series resistance and demonstrate more pronounced injection phenomena at higher voltages compared to Si material. At low voltages, the slope often reflects the recombination mechanism. This is because, at lower forward biases, recombination within the depletion region or through defect states may dominate the current. At high voltages, the slope typically represents the drift-diffusion mechanism. Here, the current is mainly driven by the drift and diffusion of carriers across the junction, and the exponential behavior of the I-V curve is more apparent. In Figures 5a) and b), if the slopes at low and high voltages differ, it suggests a transition from one dominant mechanism to another as the applied voltage increases. This transition can be key in understanding the behavior of the junction under different electrical conditions.

4. Conclusion

In summary, the electric field in a p-n junction plays a fundamental role in its operation, influencing carrier transport, device characteristics, and overall device performance. Our new model has been successfully calibrated with experimental results, revealing that the electric field value is inversely proportional to temperature in both Si and GaAs materials. in this paper demonstrates a strong alignment between the theory and our model. In figure 3 demonstrates a strong alignment between the theory and our model by minority charge density. When analyzing the I-U curve in these three cases A) p-n, B) p^+-n, and C) p-n^+, it was shown that in cases A) the correct connection from the recombination mechanism to the drift-diffusion mechanism prevails in Si and GaAs, respectively, at the values of 0-1 Volt and 0-1.5 Volt.

Conflict of interest statement
The authors declare that they have no conflict of interest in relation to this research, whether financial, personal, authorship or otherwise, that could affect the research and its results presented in this paper.

CRediT author statement: Abdullayev J.Sh.: Conceptualization, Data Curation, Writing Original Draft, Methodology, Investigation: Sapaev I.B.: Writing Review & Editing, Supervision.
The final manuscript was read and approved by all authors.

References

1 Shockley W. (1949) The Theory of p-n Junctions in Semiconductors and p-n Junction Transistors. *Bell System Technical Journal*, 28(3), 435–489. DOI: 10.1002/j.1538-7305.1949.tb03645.x.

2 Takeuchi D., Makino T., Kato H., Okushi H., Yamasaki S. (2011) Electron emission from diamond p-i-n junction diode with heavily P-doped n+ top layer. *Physica Status Solidi* (a), 208(9), 2073–2078. DOI:10.1002/pssa.201100140.

3 Pohl P., Renner F.H., Eckardt M., Schwanhäußer A., Friedrich A., Yüksekdag Ö., Gossard A. C. (2003) Enhanced recombination tunneling in GaAs pn junctions containing low-temperature-grown-GaAs and ErAs layers. *Applied Physics Letters*, 83(19), 4035-4037. DOI: 10.1063/1.1625108.

4 Goktas N.I., Wilson P., Ghukasyan A., Wagner D., McNamee S., LaPierre R.R. (2018) Nanowires for energy: A review. *Appl. Phys. Rev.*, 5 (4), 041305. DOI: 10.1063/1.5054842.

5 Qiang Zeng, Na Meng, Yulong Ma, Han Gu, Jing Zhang, Qingzhu Wei, Yawei Kuang, Xifeng Yang, Yushen Liu (2018) Two-Dimensional Modeling of Silicon Nanowires Radial Core-Shell Solar Cells. *Advances in Condensed Matter Physics*, 2018, 7203493. DOI: 10.1155/2018/7203493.

6 Shin J.C., Chanda D., Chern W., Yu K.J., Rogers J.A., Li X. (2012) Experimental Study of Design Parameters in Silicon Micropillar Array Solar Cells Produced by Soft Lithography and Metal-Assisted Chemical Etching. *IEEE Journal of Photovoltaics*, 2(2), 129–133. DOI: 10.1109/JPHOTOV.2011.2180894.

7 Pylypova O.V., Evtukh A.A., Parfenyuk P.V., Ivanov I.I., Korobchuk I.M., Havryliuk O.O., Semchuk O.Y. (2019) Electrical and optical properties of nanowires-based solar cell with radial p-n junction. *Opto-Electronics Review*, 27(2), 143–148. DOI: 10.1016/j.opelre.2019.05.003.

8 Jung J.-Y., Guo Z., Jee S.-W., Um H.-D., Park K.-T., Hyun M.S., Lee J.-H. (2010) A waferscale Si wire solar cell using radial and bulk p–n junctions. *Nanotechnology*, 21(44), 445303. DOI:10.1088/0957-4484/21/44/445303.

9 Prabhat B.N., Balamurugan K. (2021) Characteristics and Modeling of PN Junction Diode in Verilog-A Including Reverse Recovery. *Proceding of the IEEE 6th International Conference on Computing, Communication and Automation (ICCCA)*, Arad, Romania, 509 – 516. DOI: 10.1109/ICCCA52192.2021.9666261.

10 Khalid M., Raza W., Riaz S., Naseem S. (2015). Simulation and Analysis of Static and Dynamic Performance of Normally-off TIVJFET Using Sentaurus TCAD. *Materials Today: Proceedings*, 2(10), 5720–5725. DOI:10.1016/j.matpr.2015.11.117.

11 Kurbanov U., Zhumabaeva G., Dzhumanov S. (2024) New metal/superconductor-insulator transitions and their effect on high-T_C superconductivity in underdoped and optimally doped cuprates. *Eurasian Physical Technical Journal*, 21, 1(47), 21–27. DOI: 10.31489/2024No1/21-27.

12 Arefinia Z., Asgari A. (2015) Optical and electrical modeling of solar cells based on graphene/Si nanowires with radial p–i–n junctions. *Solar Energy Materials and Solar Cells*, 137, 146 – 153. DOI: 10.1016/j.solmat. 2015.01.032.

13 Ferreira, Gabriel M., Vítor Silva, Graça Minas, Susana O. Catarino (2022) Simulation Study of Vertical p–n Junction Photodiodes' Optical Performance According to CMOS Technology. *Applied Sciences*, 12, 5: 2580. DOI:10.3390/app12052580.

14 Abdullayev J.S., Sapaev, I. B. (2024) Optimization of The Influence of Temperature on The Electrical Distribution of Structures with Radial p-n Junction Structures. *East European Journal of Physics*, (3), 344-349. DOI:10.26565/2312-4334-2024-3-39.

15 Muhammed O.A., Danladi E., Boduku P.H., Tasiu J., Ahmad M.S., Usman N. (2021) Modeling and simulation of lead-free perovskite solar cell using SCAPS-1D. *East European Journal of Physics*, 2, 146-154.

16 Ali N.M., Allam N.K., Abdel Haleem A.M., Rafat N.H. (2014) Analytical modeling of the radial pn junction nanowire solar cells. *Journal of Applied Physics*, 116(2), 024308. DOI:10.1063/1.4886596.

17 Bal S.S., Basak A., Singh U.P. (2022) Numerical modeling and performance analysis of Sb-based tandem solar cell structure using SCAPS–1D. *Optical Materials*, 127, 112282.

18 Kelzenberg M.D., Boettcher S.W., Petykiewicz J.A., Turner-Evans D.B., Putnam M.C., Warren E.L., Atwater H.A. (2010). Erratum: Enhanced absorption and carrier collection in Si wire arrays for photovoltaic applications. *Nature Materials*, 9(4), 368–368. DOI:10.1038/nmat2727.

19 Shura M.W., Wagener V., Botha J.R., Wagener M C. (2012). Photoconduction spectroscopy of p-type GaSb films. *Physica B: Condensed Matter*., 407(10), 1656 – 1659. DOI: 10.1016/j.physb.2011.09.110.

AUTHORS' INFORMATION

Abdullayev, Jo`shqin Shakirovich – PhD, Senior Research, Senior Lecture, National Research University TIIAME, Tashkent, Uzbekistan; Scopus Author ID: 58258727900; ORCID iD:0000-0001-6110-6616; j.sh.abdullayev6@gmail.com

Sapaev, Ibrokhim Bayramdurdievich – PhD (Phys.), Associate professor, Head of the department «Physics and chemistry». National Research University TIIAME, Tashkent, Uzbekistan; Western Caspian University, Scientific researcher, Baku, Azerbaijan; Scopus Author ID: 56102062900; ORCID iD: 0000-0003-2365-1554; sapaevibrokhim@gmail.com